

See discussions, stats, and author profiles for this publication at: <https://www.researchgate.net/publication/43067521>

Development and Validation of ReaxFF Reactive Force Field for Hydrocarbon Chemistry Catalyzed by Nickel

ARTICLE *in* THE JOURNAL OF PHYSICAL CHEMISTRY C · MARCH 2010

Impact Factor: 4.77 · DOI: 10.1021/jp9035056 · Source: OAI

CITATIONS

80

READS

137

5 AUTHORS, INCLUDING:



[Jonathan Edward Mueller](#)

Universität Ulm

24 PUBLICATIONS 315 CITATIONS

[SEE PROFILE](#)



[Adri C.T. van Duin](#)

Pennsylvania State University

360 PUBLICATIONS 8,183 CITATIONS

[SEE PROFILE](#)



[William A. Goddard](#)

California Institute of Technology

1,332 PUBLICATIONS 68,116 CITATIONS

[SEE PROFILE](#)

Development and Validation of ReaxFF Reactive Force Field for Hydrocarbon Chemistry Catalyzed by Nickel

Jonathan E. Mueller,[†] Adri C. T. van Duin,[‡] and William A. Goddard III*,[†]

Materials and Process Simulation Center, California Institute of Technology, Pasadena, California 91125, and Department of Mechanical and Nuclear Engineering, Penn State University, University Park, Pennsylvania 16801

Received: April 16, 2009; Revised Manuscript Received: January 22, 2010

To enable the study of hydrocarbon reactions catalyzed by nickel surfaces and particles using reactive molecular dynamics on thousands of atoms as a function of temperature and pressure, we have developed the ReaxFF reactive force field to describe adsorption, decomposition, reformation and desorption of hydrocarbons as they interact with the nickel surface. The ReaxFF parameters were determined by fitting to the geometries and energy surfaces from quantum mechanics (QM) calculations for a large number of reaction pathways for hydrocarbon molecules chemisorbed onto nickel (111), (100) and (110) surfaces, supplemented with QM equations of state for nickel and nickel carbides. We demonstrate the validity and accuracy of ReaxFF by applying it to study the reaction dynamics of hydrocarbons as catalyzed by nickel particles and surfaces. For the dissociation of methyl on the (111), (100), and stepped (111) surfaces of nickel, we observe the formation of chemisorbed CH plus subsurface carbide. We observe that the (111) surface is the least reactive, the (100) surface has the fastest reaction rates, and the stepped (111) surface has an intermediate reaction rate. The importance of surface defects in accelerating reaction rates is highlighted by these results.

1. Introduction

The chemistry of hydrocarbons on nickel has been studied for several decades for scientific and technological reasons. Nickel is the primary catalyst in the steam reforming process¹ for converting methane and water into synthesis gas (carbon monoxide and hydrogen) which is then used in important industrial processes such as the Haber Bosch synthesis of ammonia and the Fischer–Tropsch formation of higher hydrocarbons.² Recently nickel has also been used extensively to catalyze the formation and growth of carbon nanotubes from hydrocarbon feedstock.³

Nickel's role as the catalyst of choice employed in industrial steam reformation has motivated a number of experimental^{4–7,2,8,9,2,4–9} and theoretical studies^{10–13} of methane adsorption to various nickel surfaces. Because the dissociative chemisorption of methane unto nickel is the rate-limiting step in the reformation process, much of the work on hydrocarbon chemistry on nickel surfaces has focused on the energetics and dynamics of methane sticking to various nickel surfaces, aiming to obtain an understanding of the physical nature of the activation barrier for this chemisorption process. Early experiments demonstrated that Ni(111) is the least reactive of the low index surfaces;¹⁴ however, because of its high stability much of the subsequent research has focused on exploring reactions on this surface.

Besides the Ni(111) surface, several studies have also examined the reactivity of the Ni(100)^{15–17} and Ni(211)^{2,16,18,19} surfaces. The Ni(211) surface is of special interest because it is the simplest surface that includes steps between Ni(111) terraces. Experimental studies have been conducted to test the effects of

step defects on chemisorption unto the Ni(111) surface by using gold, sulfur, alkali metals or other atoms^{20,21} to selectively bind to and hence deactivate step sites. These studies confirm that the reactivity of a Ni(111) surface is enhanced by the presence of step defects. Both experimental and theoretical studies show that steps not only provide a low energy barrier for the chemisorption of methane unto nickel but also catalyze the cleavage of additional carbon–hydrogen bonds and the formation of carbon–carbon bonds.

While much research has focused on the initial chemisorption process, other studies have examined the subsequent chemical processes that a methyl fragment undergoes once adsorbed.^{22–24} Vibrational spectra from high-resolution electron energy loss spectroscopy (HREELS) have been used to identify the stable species formed from the chemisorption of methane unto Ni(111) as a function of temperature.^{23,24} These studies show that methyl (CH_3) loses two H atoms when the temperature reaches 150 K to form methylidyne (CH), which dimerizes at temperatures above 250 K to form acetylene (CHCH). The effect of additional heating depends on the surface coverage. If the surface is nearly saturated, the CHCH molecules join together to form four-, six-, and eight-member rings. However, if the surface coverage is too low, then dehydrogenation takes place before the CHCH molecules are able to diffuse and find each other to form ring structures. Another study used secondary ion mass spectroscopy (SIMS) to detect methyl, methylene, and methylidyne intermediates in the Fischer–Tropsch synthesis of methane and water from carbon monoxide and hydrogen catalyzed on Ni(111) and concluded that a mechanism of sequential hydrogenation was responsible for methane production.²²

Atomistic simulations provide a useful tool for studying catalytic processes. In principle, quantum mechanics (QM) calculations (computing electron–electron interactions explicitly in the context of a background potential created by the nuclear charges) are capable of describing the forces on atoms along

* Corresponding author, wag@wag.caltech.edu.

[†] Materials and Process Simulation Center, California Institute of Technology.

[‡] Department of Mechanical and Nuclear Engineering, Penn State University.

catalyzed reaction pathways in heterogeneous systems.²⁵ In particular, density functional theory (DFT) is widely used to explore catalytic systems (ref 26 is an example of how DFT can be used to study a related system); however, in many cases the complexity of the system requires system sizes and numbers of time steps well beyond the current practical limits of QM calculations to sufficiently characterize the process of interest. Because of this, traditional molecular dynamics (MD) simulations (in which interatomic interactions are the basic quantity computed) can be used to treat much larger systems and longer time scales than DFT calculations; however, because most of the classical force fields employed in traditional MD simulations use a simple harmonic-like bond description, traditional MD simulations are unable to correctly describe chemical reactions.

There are two approaches for bridging the gap between QM and traditional MD methods. One may either look for approximations to reduce the computational cost of handling electron–electron interactions explicitly or else develop interatomic potentials which describe the results of electron–electron interactions implicitly. The former approach includes empirical tight binding (TB) methods, in which the number of electrons is reduced and the computation of at least some of the electron–electron interactions is simplified (ref 27 is an example of such a TB method applied to a related system). The conceptual advantage of a TB model is that the physics of electron–electron interactions is treated explicitly.

In contrast, the second approach utilizes chemical concepts (e.g., bond order, electronegativity, etc.) to describe the effects of electron–electron interactions, which are thus described implicitly in interatomic interactions. Along these lines, reactive force field methods—capable of describing bond formation and cleavage in MD simulations—have been developed.^{28–30} In particular, several of these have been applied to nickel (or other similar transition metals such as iron) and carbon in order to study carbon nanotube growth.^{31–37} A key limitation to many of the reactive force fields developed so far has been that they are typically designed to treat a very specific chemical system and are not easily transferred or extended beyond that system.

Here, we describe the development and application of a highly transferable reactive force field description for C/H/Ni systems, by deriving ReaxFF parameters for these atoms and their interactions. Some previously reported ReaxFF descriptions include hydrocarbons,³⁸ silicon/silicon oxide,³⁹ metals,⁴⁰ metal oxides,⁴¹ and metal hydrides,⁴² indicating the transferability of the ReaxFF concept. ReaxFF RD simulations have proved useful in studying a variety of complex chemical systems.^{43,44,39,45,39–44} Several years ago we reported on the development of a ReaxFF description for all carbon materials and their interactions with cobalt, nickel and copper atoms (i.e., a C/Ni force field primarily describing C–C and C–Ni bonding).⁴⁶ We have combined the C/Ni parameters from this ReaxFF description of carbon/nickel systems with the C/H parameters from ReaxFF description of hydrocarbons, and then extended the resulting force field to treat condensed nickel and nickel carbide phases, as well as the chemistry of hydrocarbon species on nickel surfaces. The result is a C/H/Ni ReaxFF force field with parameters describing C–C, C–H, C–Ni, H–Ni and Ni–Ni bonding, which is thus capable of modeling a wide range of hydrocarbon reactions catalyzed by nickel surfaces, particles or atoms.

To validate our ReaxFF description for hydrocarbons and nickel we have performed reactive MD simulations of the decomposition of methyl radicals on three nickel surfaces: (100), (111), and (111) with a step. The influence of steps has been

characterized both experimentally and theoretically, providing a basis for comparison with our results.

2. Theoretical Methods

2.1. QM Methods. Both periodic and cluster ab initio calculations were used to provide QM results against which to fit the ReaxFF parameters. Many of these QM results have been published previously.^{26,38,46}

As described elsewhere,²⁶ all periodic QM calculations were performed with the SeqQuest periodic DFT code and utilized the spin-polarized PBE flavor of DFT and pseudopotentials.⁴⁷ Forces were relaxed within 0.0005 Ry/bohr. Reasonably converged grid spacing and numbers of *k*-points were used. An accelerated steepest descent (ASD) geometry minimization algorithm was used to relax all structures. A nudged elastic band (NEB) procedure was used to calculate energy barriers for reactions.

All nonperiodic ab initio cluster calculations were taken from Nielson et al.⁴⁶ These calculations were performed with the B3LYP flavor of DFT as implemented in the Jaguar 5.0 program package.⁴⁸ Nickel was described with the Wadt and Hay core–valence (relativistic) effective core potential^{49–51} (treating the valence electrons explicitly) using the LACVP basis set with the valence double- ζ contraction of the basis functions, LACVP**. All electrons were used for all other elements using a modified variant of Pople et al.’s 6-31G** basis set,^{52,53} where the six d functions have been reduced to five. For the all-carbon training set the QM training set was composed from DFT/B3LYP/6-31G** calculations.

2.2. ReaxFF Reactive Force Field. ReaxFF uses the bond order/bond distance relationship introduced by Tersoff³⁰ and applied to carbon chemistry by Brenner to describe chemical reactivity.²⁸ Bond orders—summed from σ , π , and $\pi\pi$ terms—are calculated instantaneously from interatomic distances as follows

$$\text{BO}_{ij} = \text{BO}_{ij}^{\sigma} + \text{BO}_{ij}^{\pi} + \text{BO}_{ij}^{\pi\pi} = \exp\left[p_{\text{bo1}}\left(\frac{r_{ij}}{r_0^{\sigma}}\right)^{p_{\text{bo2}}}\right] + \exp\left[p_{\text{bo3}}\left(\frac{r_{ij}}{r_0^{\pi}}\right)^{p_{\text{bo4}}}\right] + \exp\left[p_{\text{bo5}}\left(\frac{r_{ij}}{r_0^{\pi\pi}}\right)^{p_{\text{bo6}}}\right] \quad (1)$$

Overcoordination and undercoordination energy penalties are then used to enforce the correct bond order. The total system energy is a sum of a several partial energy terms; these include energies related to lone pairs, undercoordination, overcoordination, valence and torsion angles, conjugation, hydrogen bonding, and van der Waals and Coulomb interactions. Thus, the total energy can be expressed as

$$E_{\text{system}} = E_{\text{bond}} + E_{\text{lp}} + E_{\text{over}} + E_{\text{under}} + E_{\text{val}} + E_{\text{pen}} + E_{\text{coa}} + E_{\text{C}_2} + E_{\text{tors}} + E_{\text{H-bond}} + E_{\text{vdWaals}} + E_{\text{Coulomb}} \quad (2)$$

Because Coulomb and van der Waals interactions are calculated between every pair of atoms, ReaxFF describes not only covalent bonds but also ionic bonds and the whole range of intermediate interactions. Charge distributions are calculated based on geometry and connectivity using the electronegativity equalization method (EEM).⁵⁴ Coulomb interactions are treated using a seventh order spline (Taper function).³⁹ To keep ReaxFF from erroneously predicting a

TABLE 1: Ni Parameters Fitted to 78 Point Ni Training Set (r_o^σ and r_{vdW} in Å; D_{ij} and D_e^σ in kcal/mol)

atom	r_o^σ	r_{vdW}	D_{ij}	α	γ_w
Ni	1.8201	1.9449	0.1880	12.1594	3.8387
bond	D_e^σ	$p_{be,1}$	$p_{ovun,1}$	$p_{be,2}$	$p_{bo,1}$
Ni–Ni	91.2220	−0.2538	0.2688	1.4651	−0.1435
					4.3908

strong triple bond in C_2 , an additional partial energy contribution is utilized as reported previously.⁴⁶

The force field parameters were optimized to the QM data using the single-parameter search optimization technique described previously.⁵⁵ Because the geometries of optimum reaction pathways in ReaxFF will not necessarily be identical to the optimum reaction pathways obtained from DFT, we focus our training on the energetics (relative energies of resting states and barriers) of reactions rather than on the forces along each pathway (only the zero forces as stationary points are relevant). In all cases, differential energies were obtained by comparing calculations performed using the same basis sets and the same functional. The full ReaxFF equations and parameters are supplied in the Supporting Information.

2.3. MD Simulations. The temperature-programmed (NVT)-MD simulations were performed using a velocity Verlet approach with a time step of 0.25 fs. A Berendsen thermostat with a damping constant of 100 fs was used for temperature control. Each MD simulation was initiated from an energy-minimized structure and was equilibrated to the simulation temperature by the thermostat prior to any reactive events being observed.

3. Results and Discussion

3.1. Force Field Development. To train the ReaxFF force field parameters to describe hydrocarbon reactions catalyzed on nickel particles, we began with the parameters from the previously published ReaxFF force field description of the interactions between carbon and nickel atoms, which has been successfully applied to the early stages of nanotube growth as catalyzed by nickel atoms,⁴⁶ and from the previously published ReaxFF description of hydrocarbons.³⁸ To obtain an accurate description of nickel catalyst particles, ReaxFF parameters relevant to Ni–Ni bonding (see Table 1) were optimized to fit heats of formation for nickel at various densities in face center cubic (fcc), body center cubic (bcc), a15, simple cubic, and diamond crystal structures as calculated with QM. For an accurate description of nickel catalyzed hydrocarbon chemistry, the ReaxFF parameters relevant to C–Ni and H–Ni bonding (Tables 2–5) were optimized to fit an extensive set of binding energies for hydrocarbons at nickel surface, subsurface, and bulk sites. Furthermore, because there are situations in which the catalyst particle is likely to form a nickel carbide, these same parameters were simultaneously optimized against heats of formation calculated from QM for Ni_3C , Ni_2C , and the B1, B2, B3, and B4 phases of NiC.

3.1.1. Hydrocarbon Interactions. The bond, angle, and torsion parameters for C, H, and C/H were determined by a fit to the previously published³⁸ hydrocarbon training set along with

additional structures relative to CNT growth.⁴⁶ Because of the importance of the graphite-like structures for studying carbon nanotube growth, the atomization energy for graphite was corrected to give 180.2 kcal/mol matching our QM value of 180.7 kcal/mol. Thus a total of 773 data points were used to fit 68 relevant C/H parameters. The results of this fit to our ReaxFF reactive force field can be found in the Supporting Information.

3.1.2. Nickel–Nickel Interactions. To ensure that ReaxFF appropriately treats nickel atoms in a range of chemical environments and configurations with different numbers of near neighbors, we trained it to reproduce the energies for expansions and compressions of a variety of nickel crystal structures obtained from QM. Although most of these structures are not experimentally realizable, it is important that ReaxFF is able to identify them as energetically unfavorable so that it avoids them in simulations by recognizing their high energy cost. ReaxFF predicts the equilibrium bcc crystal structure to be 0.41 kcal/mol higher in energy than the fcc structure in good agreement with our QM value of 0.85 kcal/mol. The a15 structure is 2.92 kcal/mol higher in energy than the fcc structure, agreeing with our QM result of 2.73 kcal/mol. The simple cubic crystal structure is significantly higher in energy, with ReaxFF giving an energy of 19.35 kcal/mol greater than the fcc structure, while QM gives 14.97 kcal/mol for this quantity. For high-energy states such as the simple cubic lattice, it is not essential that ReaxFF produces the energy exactly as long as it gives a sufficiently high energy to realize that the configuration is energetically unfavorable, because an energetically unfavorable structure is not something ReaxFF needs to know how to reproduce exactly, but merely to avoid. The diamond structure is even more unfavorable with QM showing it to be 30.22 kcal/mol higher than the fcc structure and ReaxFF giving a similarly large value of 35.25 kcal/mol. Figure 1 shows a comparison between relative energies for the expansion/compression curves of these crystal types obtained from ReaxFF and QM. The curves show good agreement between ReaxFF and QM, except for the diamond structure, which does not show a minimum in the region of interest. However, ReaxFF does reproduce both the unfavorable energy of the diamond structure relative to the other structures as well as the inner potential wall making diamond particularly unfavorable at typical nickel densities. This is an indication that additional training would be required before using ReaxFF to study low density nickel solid phases. Finally, it should also be noted that ReaxFF reproduces the cohesive energy of nickel (103.7 kcal/mol) in good agreement with experiment (102.4 kcal/mol).⁵⁶

The energy versus cell volume data for the nickel fcc lattice can also be used to compute structural properties such as the lattice constant, the density, and the bulk modulus. ReaxFF gives an equilibrium lattice spacing of 3.656 Å in good agreement with our QM result of 3.54 Å, and the experimental result of 3.524 Å.⁵⁷ This gives an equilibrium density of 7.98 g/cm³ which is in reasonable agreement with the experimental value of 8.91 g/cm³.⁵⁸ Using the Birch–Murnaghan equation of state to fourth order,⁵⁹ we obtain values for the bulk modulus of 148 GPa from the ReaxFF data and 142 GPa from the QM data. These are both in reasonable agreement with the experimental value of 180.26 GPa.⁵⁸

TABLE 2: Bond Parameters Fitted to 470 Point C/H/Ni Training Set (D_e^σ and D_e^π in kcal/mol, all other parameters are unitless)

bond	D_e^σ	D_e^π	$p_{be,1}$	$p_{ovun,1}$	$p_{be,2}$	$p_{bo,3}$	$p_{bo,4}$	$p_{bo,1}$	$p_{bo,2}$
C–Ni	83.5810	9.0383	0.2531	0.0529	1.4085	−0.1113	13.3900	−0.1436	4.5683
H–Ni	114.7566		−0.8939	0.1256	0.1054			−0.1196	5.0815

TABLE 3: Off-Diagonal Bond Parameters Fit to 470 Point C/H/Ni Training Set (D_{ij} in kcal/mol, R_{vdW} , r_o^σ , and r_o^π in Å, all other parameters are unitless)

	D_{ij}	R_{vdW}	α	r_o^σ	r_o^π
C–H	0.1188	1.4017	9.8545	1.1203	
C–Ni	0.0800	1.7085	10.0895	1.5504	1.4005
H–Ni	0.0366	1.7306	11.1019	1.2270	

TABLE 4: Selected Angle Parameters (parameters in italics were fit to 470 point C/H/Ni training set, Θ_0 in deg, all other parameters are unitless)

	Θ_0	$p_{val,1}$	$p_{val,2}$	$p_{val,7}$	$p_{val,4}$
C–Ni–C	62.5000	16.6806	0.7981	0.9630	1.0711
C–C–Ni	87.6241	12.6504	1.8145	0.6154	1.5298
Ni–C–Ni	100.0000	40.4895	1.6455	0.0100	1.7667
C–Ni–Ni	5.0994	3.1824	0.7016	0.7465	2.2665
H–H–Ni	0.0000	26.3327	4.6867	0.8177	1.0404
Ni–H–Ni	0.0000	60.0000	1.8471	0.6331	1.8931
H–Ni–Ni	30.3748	1.0000	4.8528	0.1019	3.1660
H–Ni–Ni	180.0000	−27.2489	8.3752	0.8112	1.0004
C–Ni–H	97.5742	10.9373	2.5200	1.8558	1.0000
C–H–Ni	0.0000	0.2811	1.1741	0.9136	3.8138
H–C–Ni	84.0006	45.0000	0.6271	3.0000	1.0000

TABLE 5: Torsion Parameters Fitted to 470 Point C/H/Ni Training Set (V_2 in kcal/mol, all other parameters are unitless)

	V_2	V_3	$p_{tor,1}$
Ni–C–C–Ni	44.3024	0.4000	−4.0000
H–C–C–Ni	21.7038	0.0100	−4.0000
H–C–Ni–C	5.2500	0.0100	−6.0000

Finally, ReaxFF reproduces the surface energies per surface atom for the Ni(111) and Ni(100) surfaces as 15.2 and 18.9 kcal/mol, respectively, compared to 14.7 and 20.4 kcal/mol from QM. For both surfaces these surface energies are in good agreement with experimental and other theoretical results. For the (111) surface the experimental results are 18.4⁶⁰ and 18.9 kcal/mol,⁶¹ while other results from theory are 15.4⁶² and 15.5 kcal/mol.⁶³ For the 100 surface the experimental value is 14.1 kcal/mol⁶⁴ and another theoretical result is 17.2 kcal/mol.⁶² Overall, 78 data points were used to fit the 11 parameters listed in Table 1.

3.1.3. Hydrocarbon Interactions with Atomic Nickel. To validate the ReaxFF method for interactions between nickel atoms and many hydrocarbon species, we used the metal hydrocarbon interactions previously computed from QM and used to train the ReaxFF parameters to study the early stages of carbon nanotube growth catalyzed by nickel atoms.⁴⁶ The results of this fitting to our updated ReaxFF can be found in the Supporting Information.

3.1.3.1. Nickel Carbides. The energies for expansions and compressions of several nickel carbide phases in Figure 2 show good agreement with corresponding QM calculations. Training with both stable and unstable carbide phases helps ensure that ReaxFF is able to recognize both favorable and unfavorable structures by energetically distinguishing between a variety of valence configurations.

3.1.3.2. Chemisorbed Hydrocarbons. To extend the ReaxFF method to treat interactions of hydrocarbons with nickel particles, we have trained the ReaxFF parameters against an extensive set of energies and structures from QM involving the binding of a range of hydrocarbon species to nickel surface and bulk structures. Because we believe that it is important to characterize the ability of different metal surface sites to form one, two, or three bonds with an adjacent hydrocarbon, we have

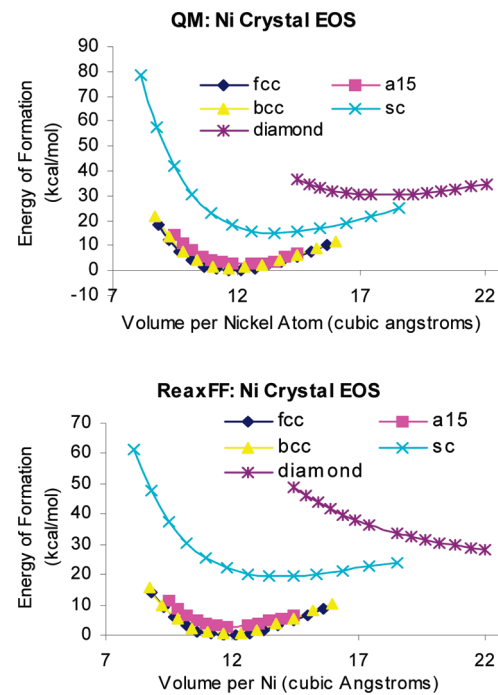


Figure 1. ReaxFF fit to EOS for various nickel crystal structures.

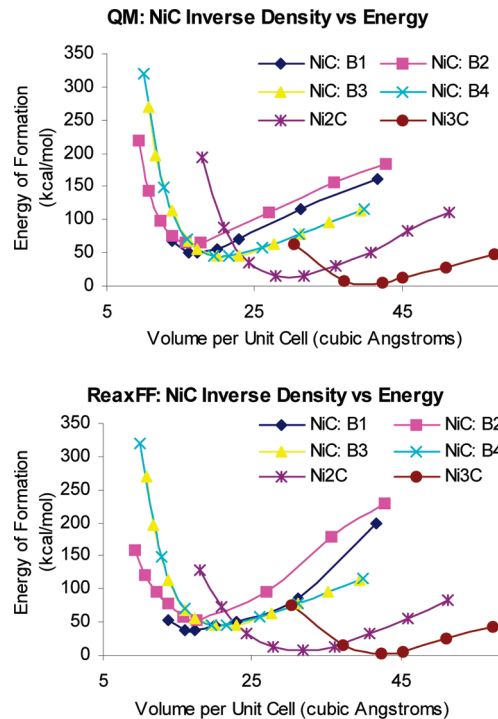


Figure 2. ReaxFF fit to EOS for various nickel carbide structures and compositions.

included the binding of H, C, CH, CH₂, and CH₃ to all surface sites (fcc, hcp, bridge, and on-top) on the nickel (111) surface. Figure 3a shows good agreement between ReaxFF and QM for heats of formation of these species bonded at these four sites.

Because C–H bond formation and cleavage are important in much of the hydrocarbon chemistry that is catalyzed by nickel particles, it is important that the ReaxFF method is able to give the appropriate barriers for C–H bond formation and cleavage in different geometric configurations on nickel. Figure 4 shows the barriers for the chemisorption and complete dissociation of CH₄ into atomic C and adsorbed H atoms on Ni(111). Because

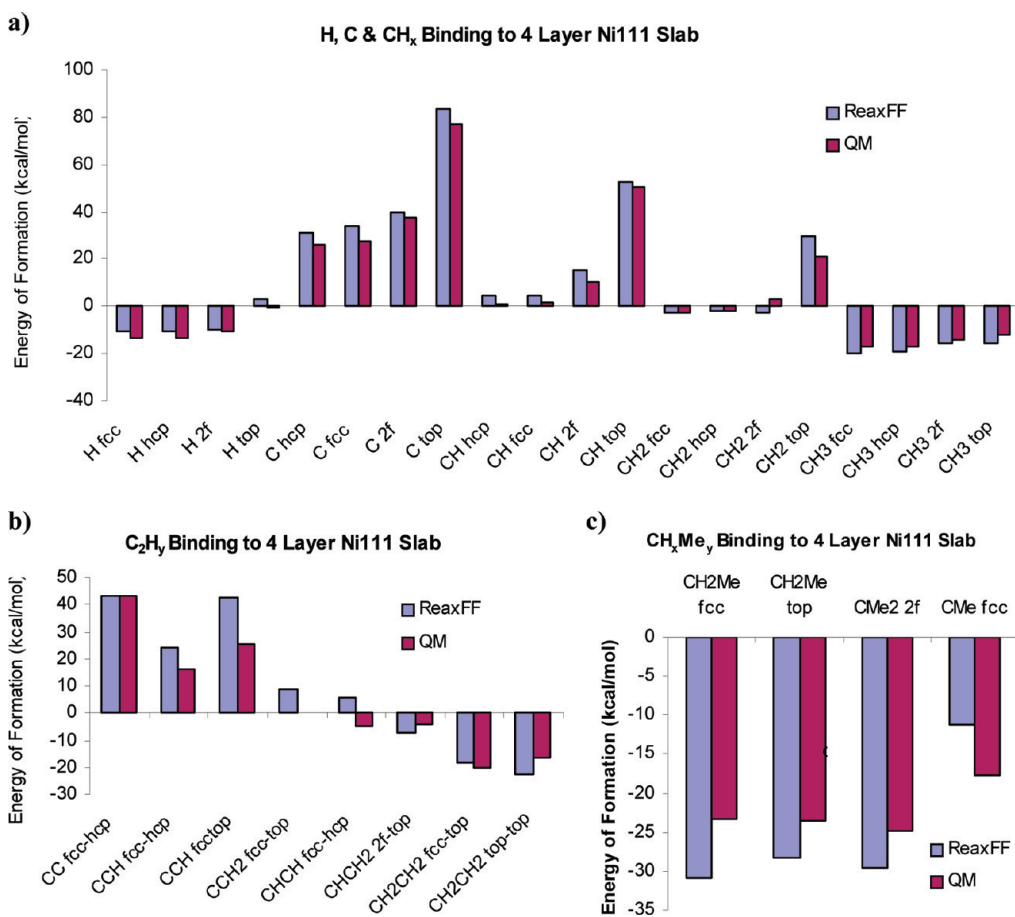


Figure 3. ReaxFF fits for (a) H, C, and CH_x binding at all Ni(111) surface sites, (b) C_2H_y species binding to Ni(111), and (c) methyl-substituted CH_x species bonded to Ni(111).

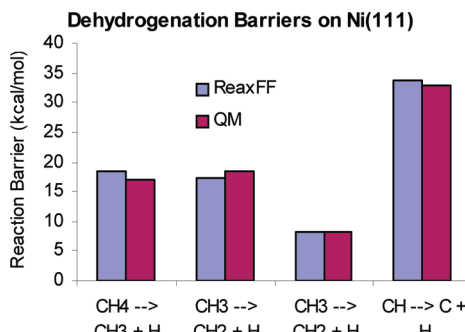


Figure 4. ReaxFF fit for barriers for methane decomposition in Ni(111).

these cases include C–H bonds pointed toward the surface ($\text{CH}_4 \rightarrow \text{CH}_3 + \text{H}$), parallel to the surface ($\text{CH}_3 \rightarrow \text{CH}_2 + \text{H}$ and $\text{CH}_2 \rightarrow \text{CH} + \text{H}$), and away from the surface ($\text{CH} \rightarrow \text{C} + \text{H}$), they demonstrate that ReaxFF is able to describe all of the basic kinds of C–H bond formation and cleavage that might take place in more complex reactions. Desorption of hydrogen from the surface as H_2 gas is also an important process for freeing surface sites and lowering the chemical potential of hydrogen on the surface. The ReaxFF parameters have also been optimized to accurately model this reaction.

Surface sites with coordination numbers not available on the (111) surface can play an important role in chemical reactions, especially when species capable of forming multiple bonds to the surface are involved. To verify that ReaxFF treats such interactions correctly, we trained it against the binding of C and CH to five coordination sites on Ni(100) and Ni(110). Comparison with QM data is in Figure 5.

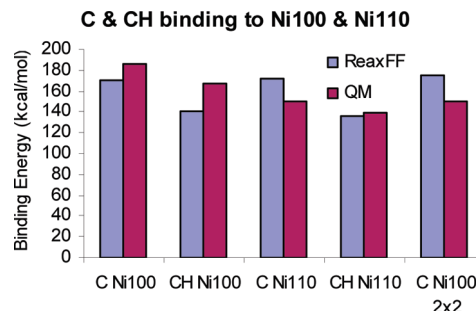


Figure 5. ReaxFF fit C and CH binding to Ni(100) and Ni(110) surfaces.

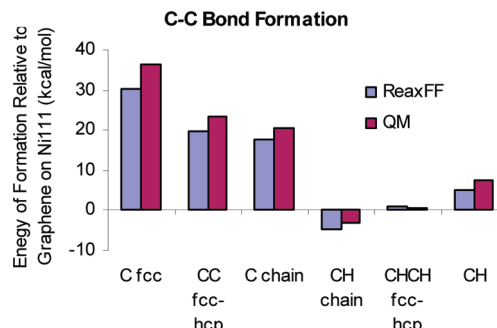


Figure 6. ReaxFF energy trends in formation of C–C bonds for extended carbon structures.

The stability of C–C bonds on nickel surfaces is important for studying both Fischer–Tropsch chemistry and the formation of carbon structures such as nanotubes on nickel catalyst

TABLE 6: Comparison of Experimental, ReaxFF, and QM Results for Binding H, CH₃, and CH to Ni(111)

	experiment	ReaxFF	QM
ΔE for $\frac{1}{2}\text{H}_{2,\text{gas}} \rightarrow \text{H}_{\text{ad}}$	-12.2 kcal/mol ⁷⁰	-10.2 kcal/mol	-13.5 kcal/mol ²⁶
ΔE^\ddagger for $\frac{1}{2}\text{H}_{2,\text{gas}} \rightarrow \text{H}_{\text{ad}}$	17.7 kcal/mol ²	18.4 kcal/mol	18.9 kcal/mol ²⁶
CH ₃ low energy site & energy preference	3-fold ²⁴	3-fold by 4.5 kcal/mol	3-fold by 3.4 kcal/mol ²⁶
CH low energy site & energy preference	3-fold ²⁴	3-fold by 10.7 kcal/mol	3-fold by 9.4 kcal/mol ²⁶

particles. The binding of CC, CCH, CCH₂, CHCH, CHCH₂, and CH₂CH₂ provides a test set that covers the complete range of carbon–carbon bond types that can be formed parallel to the surface. Figure 3b shows the energetic comparison between ReaxFF and QM for these species.

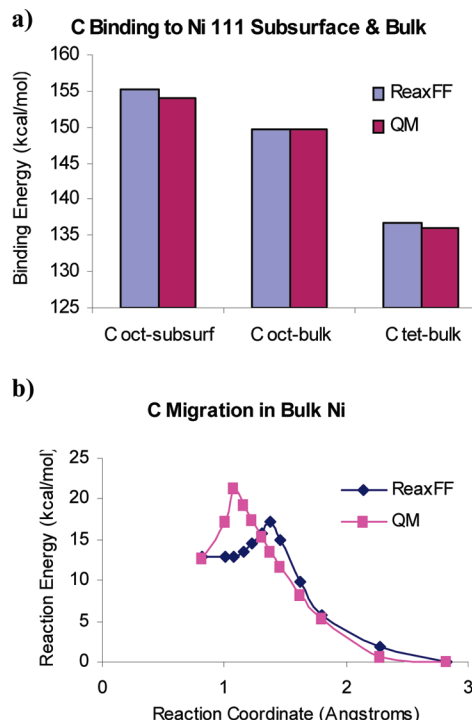


Figure 7. (a) ReaxFF fit for C in Ni bulk and subsurface binding sites. (b) ReaxFF fit to C migration between tetrahedral and octahedral interstitial sites in bulk Ni.

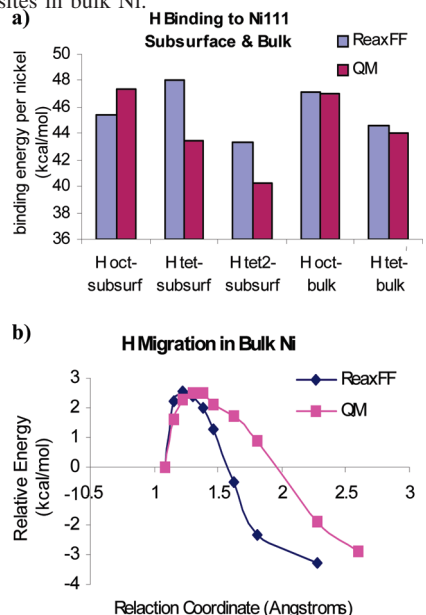


Figure 8. (a) ReaxFF fit for H in Ni bulk and subsurface binding sites. (b) ReaxFF fit to H migration between tetrahedral and octahedral interstitial sites in bulk Ni.

TABLE 7: ReaxFF Validation for Binding of Small Hydrocarbons to Ni(100) and Ni(110) Surfaces (binding energies are in kcal/mol)

	QM	ReaxFF
Binding to Ni(100)		
CH ₂ at bridge site	87.3	84.1
CH ₂ at hollow site	95.7	74.2
CH ₃ at top site	40.7	45.9
CC at adjacent top sites	124.0	84.9
CC at single hollow site	164.2	123.3
CC at adjacent hollow sites	153.4	130.5
CHCH at single hollow site	63.1	40.8
CHCH at adjacent hollow sites	46.7	47.2
CH ₂ CH ₂ at hollow site	19.5	10.3
CH ₂ CH ₂ at single top site	20.1	25.3
CH ₂ CH ₂ at adjacent top sites	18.8	22.9
Binding to Ni(110)		
CH ₂ at bridge site	86.4	86.0
CH ₃ at top site	39.5	45.6
CC at single hollow site	162.8	153.6
CC at adjacent hollow sites	148.1	152.7
CHCH at single hollow site	47.3	67.8
CHCH at adjacent hollow sites	56.0	89.1
CH ₂ CH ₂ at single top site	17.4	25.9
CH ₂ CH ₂ at adjacent top sites	19.3	28.8

Also of importance in describing the reactions of larger hydrocarbons on metal surfaces are steric interactions with the surface. To ensure that ReaxFF describes these effects correctly, the binding energies for CH_x species with methyl groups substituted for one or more of the hydrogen substituents were used to train the force field parameters. ReaxFF correctly describes these steric effects as shown in Figure 3c.

Also important for larger carbon structures is C–C bonding on nickel surfaces. Besides the many multicarbon configurations found in the all carbon training set, we trained ReaxFF to correctly describe the energies of C and CH chains on Ni(111). We have also considered the case of a graphene sheet resting on the Ni(111) surface. It is particularly important that ReaxFF reproduces the appropriate energetic trends for these species so that it correctly describes the growth of carbon structures on nickel surfaces. Figure 6 compares energies from ReaxFF and QM data for this type of process.

3.1.3.3. Subsurface and Bulk Species. Subsurface and bulk carbon is believed to be important in catalyzing processes such as nanotube growth.^{65–67} Figure 7a shows that ReaxFF correctly describes the energetics of carbon in both subsurface and bulk sites of nickel. Because carbon diffusion plays an important role in the vapor–liquid–solid (VLS) model, we included the migration barrier for interstitial carbon migration in nickel as shown in Figure 7b. Additionally, ReaxFF is capable of describing equations of state for several nickel carbide species and structures as described above.

Similarly, there are studies claiming that subsurface hydrogen can significantly alter the viable reactions that hydrocarbons on nickel surfaces are able to undergo,^{68,69} so we have also trained ReaxFF against a similar set of data for hydrogen in nickel subsurface and bulk sites. Figure 8 summarizes these results.

3.1.3.4. Charge Transfer. The EEM parameters (η , EEM hardness; χ , EEM electronegativity; and γ , EEM shielding

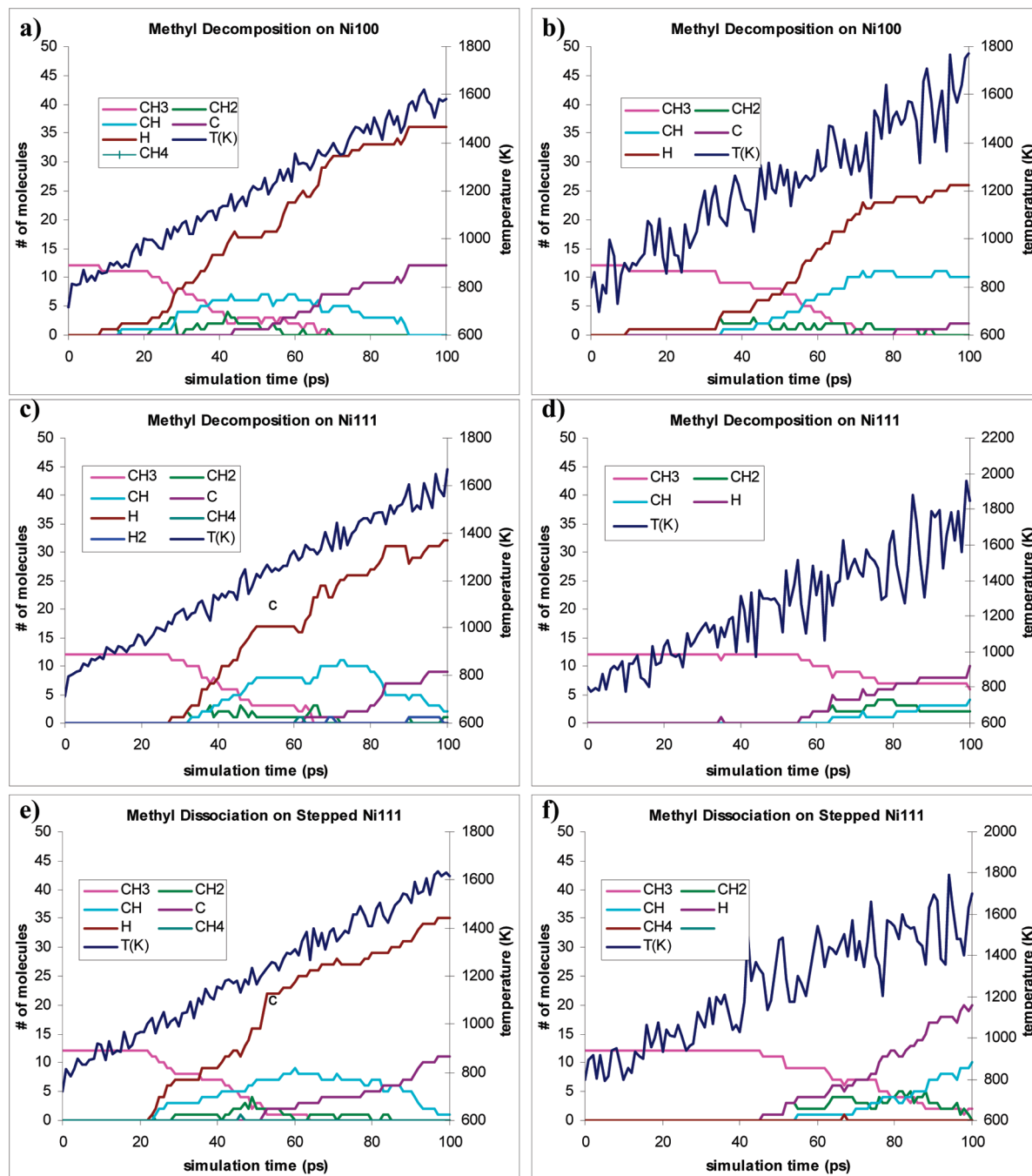


Figure 9. ReaxFF reactive MD simulations of methyl decomposition on nickel surface as the temperature is ramped from 800 to 1800 K over 100 ps. In each case there were 12 CH₃ chemisorbed at the start. For the MD on the right the nickel slab was kept at 800 K. We consider three surfaces: top row, Ni(100); central row, Ni(111); bottom row, stepped Ni(111).

parameter) for nickel were fit to Mulliken charge data from QM calculations on small clusters, with Ni in a variety of environments. For Ni bridging two CH₃ groups with single bonds, the charge on Ni is 0.0639 in ReaxFF and 0.0964 with QM. If Ni is surrounded by four CH₃ groups in a tetrahedral configuration, ReaxFF shows a charge of 0.1600 on Ni, similar to the value of 0.0700 from QM. When Ni forms a double bond to CH₂ ReaxFF finds a charge of 0.0480 on Ni (the QM value is 0.0000). In the case of binding to hydrogen there is a negative charge on Ni. Thus, for Ni bridging between two H atoms, ReaxFF gives a charge of -0.0934 on Ni compared to -0.0589 in QM.

3.1.3.5. Training Summary for C/H/Ni Parameters. In all, there are 470 data points, which 85 ReaxFF parameters relevant

to C/Ni, H/Ni, and C/H/Ni interactions were optimized to fit. These 85 parameters include 15 bond parameters (Table 2), 7 off-diagonal parameters (Table 3), 49 angle parameters (Table 4), and 9 torsion parameters (Table 5).

3.2. Force Field Validation. 3.2.1. Explicit Comparison with Experiment. While, there is very little quantitative data from experiments for explicit comparison with our ReaxFF description of C/Ni, H/Ni and C/H/Ni interactions, the following cases (summarized in Table 6) are available for consideration:

(1) The experimental activation energy for methane on Ni(111) is 17.7 kcal/mol,² the QM result we trained ReaxFF against is 18.9 kcal/mol,¹¹ and ReaxFF gives a result of 18.4 kcal/mol in excellent agreement with both.

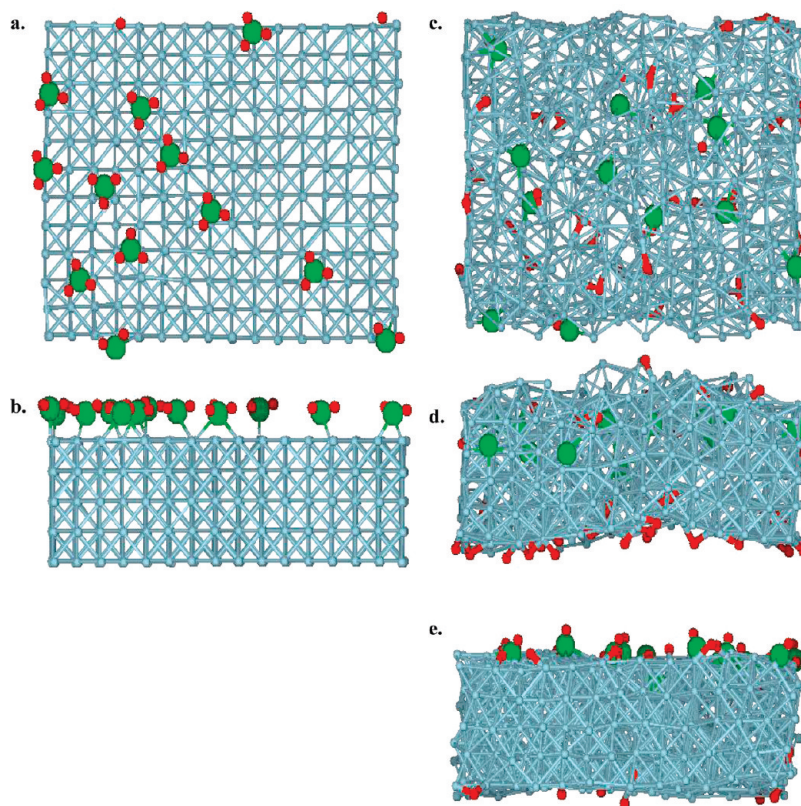


Figure 10. Snapshot of structures for ReaxFF NVT-MD simulations of methyl dissociation on Ni(100). Starting structure: (a) top view and (b) side view. Final structure (100 ps) with single thermostat: (c) top view and (d) side view. Final structure (100 ps) for simulation with nickel slab thermostat set at 800 K: (e) side view.

(2) The experimental reaction energy for $\frac{1}{2}\text{H}_2\text{gas} \rightarrow \text{H}_{\text{ad}}$ on Ni(111) is -12.2 kcal/mol (corrected to give values relative to D_e).^{70,26,26,70} The QM result we trained ReaxFF against is -13.5 kcal/mol,²⁶ and ReaxFF gives a result of -10.2 kcal/mol, which is in good agreement with both.

(3) Surface science experiments (HREELS)²⁴ suggest that a 3-fold site is the most stable binding site for both CH_3 and CH fragments on Ni(111). For CH_3 , ReaxFF finds that binding to a 3-fold (fcc) site is 4.5 kcal/mol more stable than binding to either a 1-fold (on-top) or 2-fold (bridge) site. This value is in good agreement with the values obtained from the QM results ReaxFF was trained against (5.4 and 3.4 kcal/mol, respectively). For CH ReaxFF finds that binding to a 3-fold (hcp) site is 10.7 kcal/mol lower in energy than binding to a 2-fold (bridge) site and 48.1 kcal/mol lower in energy than binding to a 1-fold (on-top) site. Again, the ReaxFF ordering matches experiment and the values agree with the QM results ReaxFF was trained against (9.4 and 49.4 kcal/mol, respectively).

3.2.2. Small Hydrocarbons Binding to Ni(100) and Ni(110). To provide further evidence for the transferability of ReaxFF to systems not explicitly included in the training set, we compare ReaxFF results for binding energies for five small hydrocarbons binding to Ni(100) and Ni(110) to results obtained from QM. The results are presented in Table 7 and show reasonable agreement between ReaxFF and QM, suggesting that although ReaxFF was trained primarily against data on hydrocarbon binding to Ni(111) that it is appropriate for applications to hydrocarbon chemistry on other nickel surfaces. These validation cases include C in a variety of chemical environments binding to several different types of nickel surface sites, again highlighting the versatility and transferability of ReaxFF.

3.2.3. MD Simulations of Methyl Decomposition. To provide additional support for the validity of using ReaxFF for

studying the decomposition of hydrocarbon molecules on nickel surfaces, we performed NVT simulations of methyl decomposition on three nickel surfaces. Each simulation started with 12 methyl radicals (CH_3) bonded to either a Ni(100) surface, a Ni(111) surface, or a Ni(111) surface with steps (one three-coordinate step and one four-coordinate step). The initial temperature was set to 800 K and increased at a rate of 10 K/ps, so that the final temperature after 100 ps of dynamics was 1800 K. As seen from the results, 800 K was an appropriate starting temperature for our simulations, because at the time scale we studied methyl decomposition is not seen below 1000 K. Our ending temperature of 1800 K is also appropriate because there is significant melting of the nickel slabs above this temperature. During each simulation the populations of hydrocarbon species formed on the surface were monitored. They are presented in parts a, c, and e of Figure 9.

On all three surfaces all or almost all of the CH_3 is converted to C and H by the end of the temperature ramp. As expected, CH_2 and CH are the key intermediates,²⁶ with CH being more stable. On Ni(100) the reaction commences at about 900 K, while on Ni(111) and stepped Ni(111) it commences at about 1000 K. In all three cases all CH_3 has decomposed by the time the temperature reaches 1300 K. The formation of CH_2 is quickly followed by further decomposition resulting in CH, so that there are never more than three or four CH_2 molecules on any surface at a given time. In contrast, CH is more stable, so that there exist simultaneously as many as 10 molecules of CH on the Ni(111) slab and seven on Ni(100) and stepped Ni(111) slabs. The CH populations are largest when the temperature is between 1100 and 1500 K. On Ni(100) all of the CH_3 is fully converted to C and H atoms by 1500 K, while a molecule or

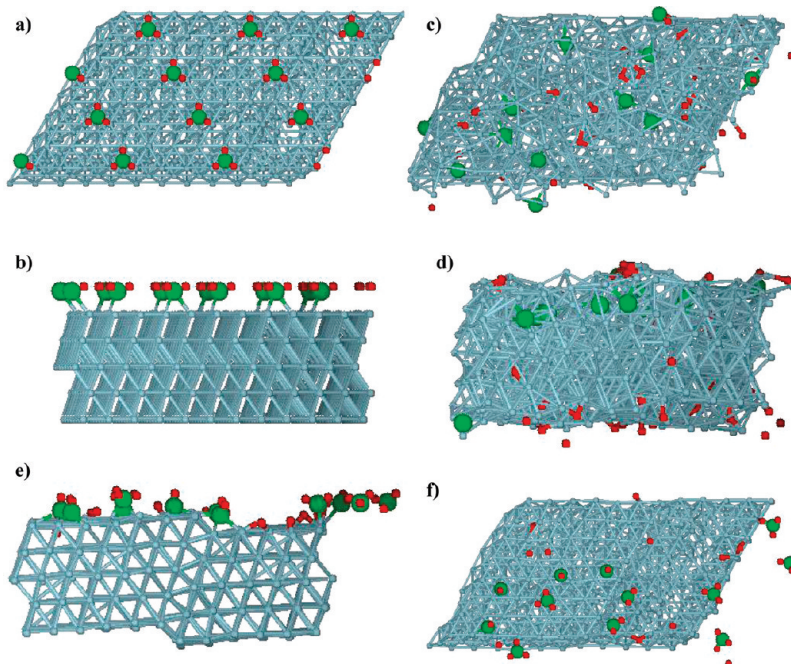


Figure 11. Snapshot of structures for ReaxFF NVT-MD simulations of methyl dissociation on Ni(111). Starting structure: (a) top view, (b) side view. Final structure (100 ps) with single thermostat: (c) top view, (d) side view. Final structure (100 ps) for simulation with nickel slab thermostat set at 800 K: (e) side view, (f) top view.

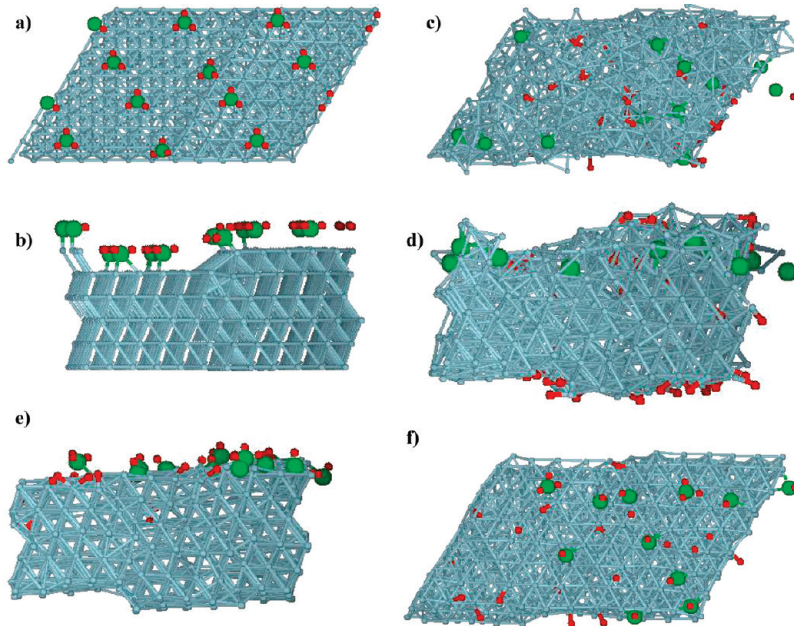


Figure 12. Snapshot of structures for ReaxFF NVT-MD simulations of methyl dissociation on stepped Ni(111). Starting structure: (a) top view, (b) side view. Final structure (100 ps) with single thermostat: (c) top view, (d) side view. Final structure (100 ps) for simulation with nickel slab thermostat set at 800 K: (e) side view, (f) top view.

two of CH remain at 1600 K on the Ni(111) and stepped Ni(111) surfaces. Thus, Ni(100) is more efficient than Ni(111) at breaking the final C–H bond to convert CH to C and H.

The final structures of these simulations are shown in Figures 10–12. A visual analysis of the trajectories reveals the following processes (see the Supporting Information for full trajectories). For the Ni(100) slab, breaking the final C–H bond to form C and H from CH is simultaneous with C going into the subsurface. Thus the C atoms formed are not adsorbed on top of the surface, but have migrated into the bulk. There is a large barrier for this to take place, which is not overcome until the temperature reaches 1250 K, 44 ps

into the simulation. When the all the CH has been converted to C and H at 90 ps (1550 K), all the C atoms produced are in the bulk of the nickel slab rather than sitting on the surface. When moved to the subsurface, C is able to form four bonds with Ni (instead of the limit of three to the surface due to geometric orbital constraints). Thus, both C and H are able to form an additional bond to Ni to compensate for the C–H bond being broken. While C prefers moving into the Ni subsurface, H prefers the surface; however, as the top surface of the slab fills up, H easily diffuses through the slab and ends up on the bottom of the slab as well. Finally, after 95 ps the Ni(100) slab begins to melt.

For Ni(111), the slab spontaneously forms a step after 20 ps. This explains the strong similarities between the Ni(111) and stepped Ni(111) slab results. The decomposition process on the Ni(111) slabs is similar to the process on Ni(100) outlined above. The key differences are a slower reaction rate (i.e., higher temperatures are required for reactions to occur on Ni(111) than on Ni(100)), especially with respect to H and C moving into the subsurface. Again, CH does not like to break down into C and H until C is able to move into an energetically more stable subsurface position. The close-packed nature of the (111) surface requires higher temperatures for surface defects capable of introducing C into the subsurface to form. Thus, C first appears in the simulation on the (100) slab at 44 ps when the temperature is less than 1250 K, while it does not appear until 63 ps in the simulation on the (111) slab, which corresponds to a temperature of 1350 K. The stepped Ni(111) surface gives results somewhere in between because the original step encourages additional surface defects to form later on.

From these simulations it appears that surface defects play an important role in speeding up CH_3 decomposition. To test the role of surface defects, we performed a second set of simulations, with two thermostats instead of one. To retain the crystalline surface structure of the slabs throughout the simulations, the temperature of the Ni atoms was maintained at 800 K, while the temperature of C and H atoms was ramped from 800 to 1800 K. Results of this second set of simulations are presented in parts b, d, and f of Figure 9. The initial and final structures can be seen in Figures 10–12. In all cases, methyl decomposition slows down significantly on the cool slabs. On the cool slabs it is much more evident that the Ni(100) surface is more reactive than the Ni(111) slab with or without steps. Of particular interest is the failure to break the final C–H bond to form C on the (111) surface and the difficulty of doing it on the (100) surface evidenced in the small number (two) of C atoms formed. This supports the hypothesis that surface defects, particularly vacancies, provide an important low energy pathway for the final dehydrogenation step.

Another noticeable difference is the absence of H migration across the cooled slabs. A couple of factors are likely involved in explaining this difference. First, the lack of defects in the Ni slab, makes it more difficult for H to find an energetically feasible pathway into the bulk. Second, a lone H in the bulk, or even on the surface, may have a difficult time maintaining its kinetic energy because it is in contact with heavier cool Ni atoms. The buildup of H on the upper surface may also be a factor in decreasing the reactivity of the cool slabs as higher surface coverage favors the formation—rather than breaking—of C–H bonds.

4. Conclusions

We find that the ReaxFF parameters developed by fitting to an extensive set of QM reaction surfaces and equations of state, lead to reactive energy surfaces for hydrocarbon decomposition, rearrangements, and reactions on nickel in good agreement with QM results. Here we have applied this ReaxFF description to explore the decomposition of methyl on Ni(100) and Ni(111) surfaces including the effect of surface defects, which we find play a substantial role in the rate of CH_3 decomposition and especially on the last step converting CH to C and H. These results are in plausible agreement with current experimental understanding of these systems, which sets the stage for using ReaxFF to study more complex reactions on nickel surfaces, as will be reported elsewhere.⁷¹ Finally, our results suggest that the ReaxFF strategy may prove useful in coupling between QM

on small systems and the large complex systems representative of the operation of real catalysts, thus, allowing reaction simulations to become useful in designing new reaction systems.

Acknowledgment. This research was supported partly by Intel Components Research and by Intel Corporate Research.

Supporting Information Available: Full ReaxFF equations, ReaxFF parameters in tabular form, ReaxFF parameters in ReaxFF format, results of ReaxFF fitting to all QM data, and trajectories for MD simulations. This material is available free of charge via the Internet at <http://pubs.acs.org>.

References and Notes

- (1) Rostrup-Nielsen, J. R. Catalytic Steam Reforming. In *Catalysis, Science and Technology*; Anderson, J. R., Boudar, M., Eds.; Springer: Berlin, 1984; p 1.
- (2) Egeberg, R. C.; Ullman, S.; Alstrup, I.; Mullins, C. B.; Chorkendorff, I. Dissociation of CH_4 on Ni(111) and Ru(0001). *Surf. Sci.* **2002**, 497 (1–3), 183–193.
- (3) Paillet, M.; Jourdain, V.; Phoncharal, P.; Sauvajol, J.-L.; Zahab, A. Versatile Synthesis of Individual Single-Walled Carbon Nanotubes from Nickel Nanoparticles for the Study of their Physical Properties. *J. Phys. Chem. B* **2004**, 108 (44), 17112–17118.
- (4) Beckerle, J. D.; Johnson, A. D.; Ceyer, S. T. Observation and Mechanism of Collision-Induced Desorption: CH_4 on Ni(111). *Phys. Rev. Lett.* **1989**, 62 (6), 685–688.
- (5) Beckerle, J. D.; Johnson, A. D.; Yang, Q. T.; Ceyer, S. T. Collision Induced Dissociative Chemisorption of CH_4 on Ni(111) by Inert Gas Atoms: The Mechanism for Chemistry with a Hammer. *J. Chem. Phys.* **1989**, 91 (9), 5756–5777.
- (6) Beckerle, J. D.; Yang, Q. T.; Johnson, A. D.; Ceyer, S. T. Collision-Induced Dissociative Chemisorption of Adsorbates: Chemistry with a Hammer. *J. Chem. Phys.* **1987**, 86 (12), 7236–7237.
- (7) Ceyer, S. T. Dissociative Chemisorption: Dynamics and Mechanisms. *Annu. Rev. Phys. Chem.* **1988**, 39, 479–510.
- (8) Lee, M. B.; Yang, Q. Y.; Tang, S. L.; Ceyer, S. T. Dynamics of the Activated Dissociative Chemisorption of CH_4 and Implication for the Pressure Gap in Catalysis: A Molecular Beam-High Resolution Electron Energy Loss Study. *J. Chem. Phys.* **1987**, 87 (1), 2724–2741.
- (9) Lee, M. B.; Yang, Q. Y.; Tang, S. L.; Ceyer, S. T. Activated Dissociative Chemisorption of CH_4 on Ni(111): Observation of a Methyl Radical and Implication for the Pressure Gap in Catalysis. *J. Chem. Phys.* **1986**, 85 (3), 1693–1694.
- (10) Burghgraef, H.; Jansen, A. P. J.; van Santen, R. A. Theoretical Investigation of CH_4 Decomposition on Ni: Electronic Structure Calculations and Dynamics. *Faraday Discuss.* **1993**, 96, 337–347.
- (11) Henkelman, G.; Arnaldsson, A.; Jonsson, H. Theoretical Calculations of CH_4 and H_2 Associative Desorption from Ni(111): Could Subsurface Hydrogen Play an Important Role? *J. Chem. Phys.* **2006**, 124 (4), 044706.
- (12) Wonchoba, S. E.; Truhlar, D. G. Embedded Diatomics-in-Molecules Potential Energy Function for Methyl Radical and Methane on Nickel Surfaces. *J. Phys. Chem. B* **1998**, 102 (35), 6842–6860.
- (13) Yang, H.; Whitten, J. L. Ab initio Chemisorption Studies of CH_3 on Ni(111). *J. Am. Chem. Soc.* **1991**, 113 (17), 6442–6449.
- (14) Beebe, T. P.; Goodman, D. W.; Kay, B. D.; Yates, J. D. Kinetics of the Activated Dissociative Adsorption of Methane on the Low Index Planes of Nickel Single Crystal Surfaces. *J. Chem. Phys.* **1987**, 87 (4), 2305–2315.
- (15) Abbott, H. L.; Burkoski, A.; Kavulak, D. F.; Harrison, I. Dissociative Chemisorption of Methane on Ni(100): Threshold Energy from $\text{CH}_4(2\nu_3)$ Eigenstate-Resolved Sticking Measurements. *J. Chem. Phys.* **2003**, 119 (13), 6407–6410.
- (16) Bengaard, H. S.; Alstrup, I.; Chorkendorff, I.; Ullmann, S.; Rostrup-Nielsen, J. R.; Nørskov, J. K. Chemisorption of Methane on Ni(100) and Ni(111) Surfaces with Preadsorbed Potassium. *J. Catal.* **1999**, 187 (1), 238–244.
- (17) Lai, W. Z.; Xie, D. Q.; Zhang, D. H. First-Principles Study of Adsorption of Methyl, Coadsorption of Methyl and Hydrogen, and Methane Dissociation on Ni(100). *Surf. Sci.* **2005**, 594 (1–3), 83–92.
- (18) Abild-Pedersen, F.; Lytken, O.; Engbaek, J.; Nielsen, G.; Chorkendorff, I.; Nørskov, J. K.; et al. Methane Activation on Ni(111): Effects of Poisons and Step Defects. *Surf. Sci.* **2005**, 590 (2–3), 127–137.
- (19) Kratzer, P.; Hammer, B.; Nørskov, J. K. A Theoretical Study of CH_4 Dissociation on Pure and Gold-Alloyed Ni(111) Surfaces. *J. Chem. Phys.* **1996**, 105 (13), 5595–5604.
- (20) Bengaard, H. S.; Nørskov, J. K.; Sehested, J.; Clausen, B. S.; Nielsen, L. P.; Molenbroek, A. M.; Rostrup-Nielsen, J. R. Steam Reforming and Graphite Formation on Ni Catalysts. *J. Catal.* **2002**, 209 (2), 365–384.

- (21) Hofmann, S.; Sharma, R.; Ducati, C.; Du, G.; Mattevi, C.; Cepek, C.; Cantoro, M.; Pisana, S.; Parvez, A.; Cervantes-Sodi, F.; Ferrari, A. C.; Dunin-Borkowski, R.; Lizzit, S.; Petaccia, L.; Goldoni, A.; Robertson, J. In situ Observations of Catalyst Dynamics During Surface-Bound Carbon Nanotube Nucleation. *Nano Lett.* **2007**, *7* (3), 602–608.
- (22) Kaminsky, M. P.; Winograd, N.; Geoffroy, G. L.; Vannice, M. A. Direct SIMS Observation of Methylidyne, Methylene, and Methyl Intermediates on a Ni(111) Methanation Catalyst. *J. Am. Chem. Soc.* **1986**, *108* (6), 1315–1316.
- (23) Yang, Q. Y.; Ceyer, S. T. The Stability and Chemistry of Methyl Radicals Adsorbed on Ni(111). *J. Vac. Sci. Technol., A* **1988**, *6* (3), 851–852.
- (24) Yang, Q. Y.; Maynard, K. J.; Johnson, A. D.; Ceyer, S. T. The Structure and Chemistry of CH₃ and CH Radicals Adsorbed on Ni(111). *J. Chem. Phys.* **1995**, *102* (19), 7734–7749.
- (25) Car, R.; Parrinello, M. Unified Approach for Molecular Dynamics and Density Functional Theory. *Phys. Rev. Lett.* **1985**, *55* (22), 2471–2474.
- (26) Mueller, J. E.; van Duin, A. C. T.; Goddard, W. A. Structures, Energetics, and Reaction Barriers for CH_x Bound to Ni(111) Surfaces. *J. Phys. Chem. C* **2009**, *113* (47), 20290–20306.
- (27) Amara, H.; Roussel, J.-M.; Bichara, C.; Gaspard, J.-P.; Ducastelle, F. Tight-Binding Potential for Atomistic Simulations of Carbon Interacting with Transition Metals: Application to the Ni-C System. *Phys. Rev. B* **2009**, *79* (1), 014109.
- (28) Brenner, D. W. Empirical Potential for Hydrocarbons for Use in Simulating the Chemical Vapor-Deposition of Diamond Films. *Phys. Rev. B* **1990**, *42* (15), 9458–9471.
- (29) Brenner, D. W.; Shenderova, O. A.; Harrison, J. A.; Stuart, S. J.; Ni, B. A Second-Generation Reactive Empirical Bond Order (REBO) Potential Energy Expression for Hydrocarbons. *J. Phys.: Condens. Matter* **2002**, *14* (4), 783–802.
- (30) Tersoff, J. Empirical Interatomic Potential for Carbon, with Applications to Amorphous-Carbon. *Phys. Rev. Lett.* **1988**, *61* (25), 2879–2882.
- (31) Ding, F.; Bolton, K.; Rosen, A. Nucleation and Growth of Single-Walled Carbon Nanotubes: A Molecular Dynamics Study. *J. Phys. Chem. B* **2004**, *108* (45), 17369–17377.
- (32) Ding, F.; Rosen, A.; Bolton, K. Molecular Dynamics Study of the Catalyst Particle Size Dependence on Carbon Nanotube Growth. *J. Chem. Phys.* **2004**, *121* (6), 2775–2779.
- (33) Ding, F.; Rosen, A.; Bolton, K. The Role of the Catalytic Particle Temperature Gradient for SWNT Growth from Small Particles. *Chem. Phys. Lett.* **2004**, *393* (4–6), 309–313.
- (34) Maiti, A.; Brabec, C. J.; Bernholc, J. Kinetics of Metal-Catalyzed Growth of Single-Walled Carbon Nanotubes. *Phys. Rev. B* **1997**, *55* (10), R6097–R6100.
- (35) Maiti, A.; Brabec, C. J.; Roland, C.; Bernholc, J. Theory of Carbon Nanotube Growth. *Phys. Rev. B* **1995**, *52* (20), 14850–14858.
- (36) Shibuta, Y.; Maruyama, S. Molecular Dynamics Simulation of Formation Process of Single-Walled Carbon Nanotubes by CCVD Method. *Chem. Phys. Lett.* **2003**, *382* (3–4), 381–386.
- (37) Shibuta, Y.; Maruyama, S. Molecular Dynamics Simulation of Generation Process of SWNTs. *Phys. B (Amsterdam, Neth.)* **2002**, *323* (1–4), 187–189.
- (38) van Duin, A. C. T.; Dasgupta, S.; Lorant, F.; Goddard, W. A. ReaxFF: A Reactive Force Field for Hydrocarbons. *J. Phys. Chem. A* **2001**, *105* (41), 9396–9409.
- (39) van Duin, A. C. T.; Strachan, A.; Stewman, S.; Zhang, Q.; Xu, X.; Goddard, W. A. ReaxFF_{SiO} Reactive Force Field for Silicon and Silicon Oxide Systems. *J. Phys. Chem. A* **2003**, *107* (19), 3803–3811.
- (40) Zhang, Q.; Cagin, T.; van Duin, A. C. T.; Goddard, W. A.; Qi, Y.; Hector, L. G. Adhesion and Nonwetting-Wetting Transition in the Al/α-Al₂O₃ Interface. *Phys. Rev. B* **2004**, *69* (4), 045423.
- (41) Chenoweth, K.; van Duin, A. C. T.; Persson, P.; Cheng, M.-J.; Osgaard, J.; Goddard, W. A. Development and Application of a ReaxFF Reactive Force Field for Oxidative Dehydrogenation on Vanadium Oxide Catalysts. *J. Phys. Chem. C* **2008**, *112* (37), 14645–14654.
- (42) Cheung, S.; Deng, W.-Q.; van Duin, A. C. T.; Goddard, W. A. ReaxFF_{MgH} Reactive Force Field for Magnesium Hydride Systems. *J. Phys. Chem. A* **2005**, *109* (5), 851–859.
- (43) Chenoweth, K.; Cheung, S.; van Duin, A. C. T.; Goddard, W. A.; Kober, E. M. Simulations on the Thermal Decomposition of a Poly(dimethylsiloxane) Polymer Using the ReaxFF reactive Force Field. *J. Am. Chem. Soc.* **2005**, *127* (19), 7192–7202.
- (44) Chenoweth, K.; van Duin, A. C. T.; Goddard, W. A. ReaxFF Reactive Force Field for Molecular Dynamics Simulations of Hydrocarbon Oxidation. *J. Phys. Chem. A* **2008**, *112* (5), 1040–1053.
- (45) van Duin, A. C. T.; Faina, Y. Z.; Dubnikova, F.; Kosloff, R.; Goddard, W. A. Atomistic-Scale Simulations of the Initial Chemical Events in the Thermal Initiation of Triacetone-tri-peroxide. *J. Am. Chem. Soc.* **2005**, *127* (31), 11053–11062.
- (46) Nielson, K. D.; van Duin, A. C. T.; Osgaard, J.; Deng, W. Q.; Goddard, W. A. Development of the ReaxFF Reactive Force Field for Describing Transition Metal Catalyzed Reactions, with Application to the Initial Stages of the Catalytic Formation of Carbon Nanotubes. *J. Phys. Chem. A* **2005**, *109* (3), 493–499.
- (47) Schultz, P. A. *SeqQuest*; Sandia National Labs: Albuquerque, NMhttp://dft.sandia.gov/Quest/.
- (48) *Jaguar*; Schrodinger, Inc.: Portland, OR, 2000.
- (49) Goddard, W. A. New Foundation for Use of Pseudopotentials in Metals. *Phys. Rev.* **1968**, *174* (3), 659–662.
- (50) Hay, P. J.; Wadt, W. R. Ab initio Effective Core Potentials for Molecular Calculations: Potentials for K to Au Including the Outermost Core Orbitals. *J. Chem. Phys.* **1985**, *82* (1), 299–310.
- (51) Melius, C. F.; Olafson, B. D.; Goddard, W. A. Fe and Ni Ab initio Effective Potentials for Use in Molecular Calculations. *Chem. Phys. Lett.* **1974**, *28* (4), 457–462.
- (52) Franchi, M. M.; Pietro, W. J.; Hehre, W. J.; Binkley, J. S.; Gordon, M. S.; Defrees, D. J.; Pople, J. A. Self-Consistent Molecular Orbital Methods. XXIII. A Polarization-Type Basis Set for Second-Row Elements. *J. Chem. Phys.* **1982**, *77* (7), 3654–3665.
- (53) Hariharan, P. C.; Pople, J. A. Effect of d-Functions on Molecular-Orbital Energies for Hydrocarbons. *Chem. Phys. Lett.* **1972**, *16* (2), 217–219.
- (54) Mortier, W. J.; Ghosh, S. K.; Shankar, S. Electronegativity Equalization Method for the Calculation of Atomic Charges in Molecules. *J. Am. Chem. Soc.* **1986**, *108* (15), 4315–4320.
- (55) van Duin, A. C. T.; Baas, J. M. A.; van de Graaf, B. Delft Molecular Mechanics: A New Approach to Hydrocarbon Force Fields. *J. Chem. Soc., Faraday Trans.* **1994**, *90* (19), 2881–2895.
- (56) Kittel, C. *Introduction to Solid State Physics*, 8th ed.; Wiley: New York, 2005.
- (57) Massabki, T. B. ed. *Binary Alloy Phase Diagrams*. 1986, Metals Park, OH: ASM International.
- (58) *Handbook of Physical Quantities*; Grigoriev, I. S., Ed.; CRC Press: New York, 1997.
- (59) Birch, F. Finite Elastic Strain of Cubic Crystals. *Phys. Rev.* **1947**, *71* (11), 809–824.
- (60) Tyson, W. R.; Miller, W. A. Surface Free Energies of Solid Metals: Estimation from Liquid Surface-Tension Measurements. *Surf. Sci.* **1977**, *62* (1), 267–276.
- (61) de Boer, F. R.; Boom, R.; Matteris, W. C. M.; Miedema, A. R.; Niessen, A. K. *Cohesion in Metals*; North-Holland: Amsterdam, 1988.
- (62) Hong, S.; Shin, Y.-H.; Ihm, J. Crystal Shape of a Nickel Particle Related to Carbon Nanotube Growth. *Jpn J. Appl. Phys.* **2002**, *41*, 6142.
- (63) Kalibaeva, G.; Vuilleumier, R.; Meloni, S.; Alavi, A.; Ciccotti, G.; Rosei, R. Ab Initio Simulation of Carbon Clustering on an Ni(111) Surface: A Model of the Poisoning of Nickel-Based Catalysts. *J. Phys. Chem. B* **2006**, *110* (8), 3638–3646.
- (64) Maiya, P. S.; Blakely, J. M. Surface Self-Diffusion and Surface Energy of Nickel. *J. Appl. Phys.* **1967**, *38* (2), 698–704.
- (65) Rodriguez-Manzo, J. A.; Terrones, M.; Terrones, H.; Kroto, H. W.; Sun, L.; Banhart, F. In situ Nucleation of Carbon Nanotubes by the Injection of Carbon Atoms into Metal Particles. *Nat. Nanotechnol.* **2007**, *2* (5), 307–311.
- (66) Saito, Y. Nanoparticles and Filled Nanocapsules. *Carbon* **1995**, *33* (7), 979–988.
- (67) Wagner, R. S.; Ellis, W. C. Vapor-Liquid-Solid Mechanism of Single Crystal Growth. *Appl. Phys. Lett.* **1964**, *4* (5), 89–.
- (68) Daley, S. P.; Utz, A. L.; Trautman, T. R.; Ceyer, S. T. Ethylene Hydrogenation on Ni(111) by Bulk Hydrogen. *J. Am. Chem. Soc.* **1994**, *116* (13), 6001–6002.
- (69) Johnson, A. D.; Daley, S. P.; Utz, A. L.; Ceyer, S. T. The Chemistry of Bulk Hydrogen: Reaction of Hydrogen Embedded in Nickel with Adsorbed CH₃. *Science* **1992**, *257* (5067), 223–225.
- (70) Christmann, K.; Behm, R. J.; Ertl, G.; van Hove, M. A.; Weinberg, W. H. Chemisorption Geometry of Hydrogen on Ni(111): Order and Disorder. *J. Chem. Phys.* **1979**, *70* (9), 4168–4184.
- (71) Mueller, J. E.; van Duin, A. C. T.; Goddard, W. A. Application of the ReaxFF Reactive Force Field to Reactive Dynamics of Hydrocarbon Chemisorption and Decomposition. *J. Phys. Chem. C* **2010**, published online January 27, 2010, http://dx.doi.org/10.1021/jp9089003.